Reentrant Correlated Insulators in Twisted Bilayer Graphene at 25 T (math xmlns="http://www.w3.org/1998/Math/MathML" display="inline">mn>2/mn>mi>π/mi>/math> Flux)

Jonah Herzog-Arbeitman, Aaron Chew, Dmitri K. Efetov, and B. Andrei Bernevig

Phys. Rev. Lett. **129**, 076401 — Published 9 August 2022

DOI: 10.1103/PhysRevLett.129.076401

Reentrant Correlated Insulators in Twisted Bilayer Graphene at 25T (2π Flux)

Jonah Herzog-Arbeitman[1], Aaron Chew[1], Dmitri K. Efetov[2], and B. Andrei Bernevig[1,3,4]
[1]*Department of Physics, Princeton University, Princeton, NJ 08544*
[2] *ICFO - Institut de Ciencies Fotoniques, The Barcelona Institute of Science and Technology, Castelldefels, Barcelona 08860, Spain*
[3]*Department of Physics, Princeton University, Princeton, NJ 08544*
Donostia International Physics Center, P. Manuel de Lardizabal 4, 20018 Donostia-San Sebastian, Spain and
[4]*IKERBASQUE, Basque Foundation for Science, Bilbao, Spain*
(Dated: July 12, 2022)

Twisted bilayer graphene (TBG) is remarkable for its topological flat bands, which drive strongly-interacting physics at integer fillings, and its simple theoretical description facilitated by the Bistritzer-MacDonald Hamiltonian, a continuum model coupling two Dirac fermions. Due to the large moiré unit cell, TBG offers the unprecedented opportunity to observe reentrant Hofstadter phases in laboratory-strength magnetic fields near 25T. This Letter is devoted to magic-angle TBG at 2π flux where the magnetic translation group commutes. We use a newly developed gauge-invariant formalism to determine the exact single-particle band structure and topology. We find that the characteristic TBG flat bands reemerge at 2π flux, but, due to the magnetic field breaking $C_{2z}\mathcal{T}$, they split and acquire Chern number ± 1. We show that reentrant correlated insulating states appear at 2π flux driven by the Coulomb interaction at integer fillings, and we predict the characteristic Landau fans from their excitation spectrum.

Introduction. Twisted bilayer graphene (TBG) is the prototypical moiré material obtained from rotating two graphene layers by an angle θ. Near the magic-angle $\theta = 1.05°$, the two bands near charge neutrality flatten to a few meV, pushing the system into the strong-coupling regime featuring correlated insulators and superconductors [1–7]. Due to the large moiré unit cell, magnetic fluxes of 2π are achieved at only 25T. In Hofstadter tight-binding models with the Peierls substitution, e.g. the square lattice, the 2π-flux and zero-flux models are equivalent, although the situation is more complicated in TBG [8]. This begs the question: do insulating and superconducting phases of TBG repeat at 25T?

We study the Bistritzer-MacDonald (BM) Hamiltonian [9], describing the interlayer moiré-scale coupling of the graphene Dirac fermions within a single valley. We write the BM Hamiltonian (neglecting $O(\theta)$ terms) as

$$H_{BM}(\mathbf{r}) = \begin{pmatrix} -i\hbar v_F \boldsymbol{\nabla}\cdot\boldsymbol{\sigma} & h.c. \\ \sum_{j=1}^{3} T_j e^{2\pi i \mathbf{q}_j\cdot\mathbf{r}} & -i\hbar v_F \boldsymbol{\nabla}\cdot\boldsymbol{\sigma} \end{pmatrix} . \tag{1}$$

Here $\mathbf{q}_j = C_{3z}^{j-1}\mathbf{q}_1$ are the inter-layer momentum hoppings, $\mathbf{q}_1 = (0, 4\sin(\frac{\theta}{2})/3a_g)$, and $a_g = .246$nm is the graphene lattice constant. The BM couplings $T_1 = w_0\sigma_0 + w_1\sigma_1$, $T_{j+1} = \exp(\frac{2\pi i}{3} j\sigma_3) T_1 \exp(-\frac{2\pi i}{3} j\sigma_3)$ act on the sublattice indices of the Dirac fermions, and σ_j are the Pauli matrices. The lattice potential scale is $w_1 = 110$meV with $w_0/w_1 = .6$ - $.8$ [10, 11] and the kinetic energy scale is $2\pi\hbar v_F|\mathbf{q}_1| = 190$meV. The spectrum of $H_{BM}(\mathbf{r})$ has been thoroughly investigated [12–17].

The salient feature of the BM model from the Hofstadter perspective is the size of the moiré unit cell. After a unitary transform by $\mathrm{diag}(e^{i\pi\mathbf{q}_1\cdot\mathbf{r}}, e^{-i\pi\mathbf{q}_1\cdot\mathbf{r}})$, $H_{BM}(\mathbf{r})$ is put into Bloch form and is periodic under translations by $\mathbf{a}_i$, the moiré lattice vectors [18]. Near the magic-angle, the moiré unit cell area $\Omega = |\mathbf{a}_1 \times \mathbf{a}_2|$ is a factor of $\theta^{-2} \sim 3000$ times larger than the graphene unit cell. This dramatic increase in size brings the Hofstadter regime

$$\phi = eB\Omega/\hbar \sim 2\pi \tag{2}$$

within reach, showcasing physics which is only possible in strong flux [8, 19–24]. Here $e/2\pi\hbar$ is the flux quantum (henceforth $e = \hbar = 1$) and the magnetic field B is near 25T at $\phi = 2\pi$ and $\theta = 1.05°$. Although there is not an exact 2π periodicity in flux, we will show that the flat bands and correlated insulators are revived at $\phi = 2\pi$.

A constant magnetic field $\epsilon_{ij}\partial_i A_j = B > 0$ (repeated indices are summed) is incorporated into Eq. (1) via the canonical substitution $-i\boldsymbol{\nabla} \to \boldsymbol{\pi} = -i\boldsymbol{\nabla} - \mathbf{A}(\mathbf{r})$ yielding H^{ϕ}_{BM}. Because $\mathbf{A}(\mathbf{r})$ breaks translation symmetry, the spectrum in flux cannot be solved using Bloch's theorem. This problem has a long history with many approaches [25–38], most frequently relying on the Landau gauge. However, an understanding of TBG in flux requires more than just the spectrum. To rigorously derive expressions for the Wilson loop and many-body form factors at 2π flux, we employ a newly developed gauge-invariant formalism [39] built from the magnetic translation group. We apply the theory here to study the single-particle and many-body physics of TBG at 2π flux. Accompanying this paper, Ref. [40] experimentally confirms our prediction of re-entrant correlated insulators at 2π flux.

Magnetic Bloch Theorem. In zero flux, the translation group of a crystal allows one to construct an orthonormal basis of momentum eigenstates labeled by $\mathbf{k}$ in the Brillouin zone (BZ) and the spectrum is given by the Bloch Hamiltonian at each $\mathbf{k}$. A similar construction can be followed at 2π flux where the magnetic translation group commutes and is isomorphic to the zero-flux translation group. As detailed in Ref. [39], we construct irreps at $\phi = 2\pi$, valid in any gauge, in the form

$$|\mathbf{k}, n, \alpha, l\rangle = \frac{1}{\sqrt{\mathcal{N}(\mathbf{k})}} \sum_{\mathbf{R}} e^{-i\mathbf{k}\cdot\mathbf{R}} T_{\mathbf{a}_1}^{\mathbf{R}\cdot\mathbf{b}_1} T_{\mathbf{a}_2}^{\mathbf{R}\cdot\mathbf{b}_2} |n, \alpha, l\rangle \tag{3}$$

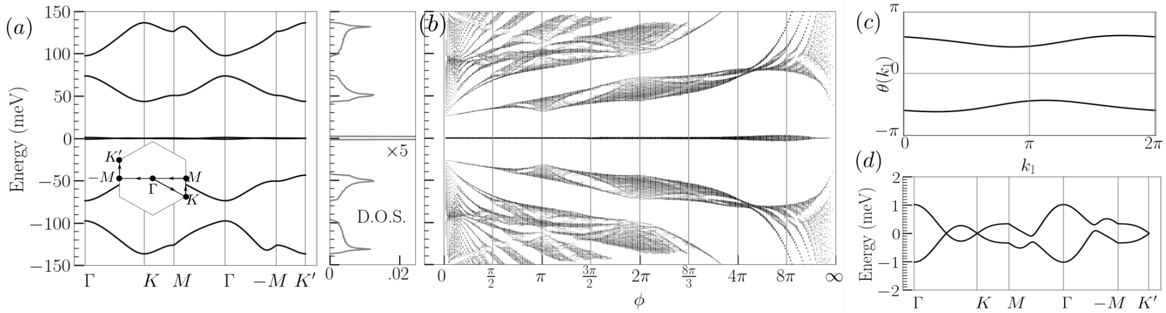

FIG. 1. TBG in flux. (a) The band structure and density of states at $\phi = 2\pi$, $w_0/w_1 = 0.8$, and $\theta = 1.05^\circ$ reveal ~ 1.5meV flat bands with a 40meV gap. (b) The Hofstadter spectrum shows the flat bands remain gapped at all flux. (c) The Wilson loop of the two flat bands is trivial due to $C_2\mathcal{T}$ breaking when particle-hole symmetry is intact. (d) The flat bands at 2π flux.

where $\mathbf{R}$ is the moiré Bravais lattice, $\alpha = 1, \dots, 4$ is the composite sublattice/layer index, and n is the Landau level defined by $|n,\alpha\rangle = \frac{a^{\dagger\, n}}{\sqrt{n!}} |0,\alpha\rangle$, $a|0,\alpha\rangle = 0$ with $a, a^\dagger$ the Landau level operators [41]. The states in Eq. (3) are orthogonal, periodic, and obey $T_{\mathbf{a}_i} |\mathbf{k}, n, \alpha\rangle = e^{i\mathbf{k}\cdot\mathbf{a}_i} |\mathbf{k}, n, \alpha\rangle$ where $T_{\mathbf{a}_i}$ are the magnetic translation operators at 2π flux. The normalization $\mathcal{N}(\mathbf{k})$ can be expressed in terms of theta functions [41] and is responsible for encoding the topology of the underlying Landau levels in momentum space. With the basis states in Eq. (3), we can diagonalize the Hamiltonian at each $\mathbf{k}$ to produce a band structure. As computed in Fig. 1a, the famous flat bands of magic-angle TBG reappear at 2π flux. We use the open momentum space technique [38] to obtain the Hofstadter spectrum (Fig. 1b) which shows the evolution of the higher energy passive bands. Despite splitting into Hofstadter bands at rational flux, the density of states remains strongly confined all the way up to 2π flux where full density Bloch-like flat bands reemerge.

Topology of the Flat bands. Similar to the zero flux TBG flat bands, the reentrant flat bands at 2π flux have a very small bandwidth of ~ 1 meV. However, their topology is quite different due to the breaking of crystalline symmetries by magnetic field. Let us review the zero flux model. Ref. [12] showed that the space group $p6'2'2$ of the BM Hamiltonian (Eq. (1)) was generated by C_{3z}, C_{2x}, and $C_{2z}\mathcal{T}$ and also featured an approximate unitary particle-hole operator P. Notably, $C_{2z}\mathcal{T}$ alone is sufficient to protect the gapless Dirac points and fragile topology of the flat bands [12]. Because a perpendicular magnetic field is reversed by time-reversal and C_{2x} (while it is invariant under in-plane rotations), C_{2x} and $C_{2z}\mathcal{T}$ are broken for all nonzero flux [8]. Thus, the space group of H^ϕ_{BM} is reduced to $p31m'$ which is generated by C_{3z} and $M\mathcal{T} \equiv C_{2x}C_{2z}\mathcal{T}$. P also remains a symmetry.

Without $C_{2z}\mathcal{T}$, the system changes substantially. The most direct way to assess the topology at 2π flux is to calculate the non-Abelian Wilson loop. To do so, we need an expression for the Berry connection $\mathcal{A}^{MN}(\mathbf{k})$ where M, N index the occupied bands. At 2π flux, the Berry connection $\mathcal{A}_i = \mathbf{b}_i \cdot \mathcal{A}$ contains new contributions [39]:

$$\begin{aligned} \mathcal{A}_i^{MN}(\mathbf{k}) = [U^\dagger(\mathbf{k})(i\partial_{k_i} - \epsilon_{ij}\tilde{Z}_j)U(\mathbf{k})]^{MN} \\ - \delta^{MN}\epsilon_{ij}\partial_{k_j} \log\sqrt{\mathcal{N}(\mathbf{k})} \end{aligned} \tag{4}$$

where $U(\mathbf{k})$ is a matrix whose columns are the flat band eigenvectors. The Abelian term in the second line of Eq. (4) is an exact expression for the Berry connection of a Landau level and accounts for the Chern number of the basis states [39]. The non-Abelian term $\tilde{Z}_j$ acts on the Landau level indices [41]. We numerically calculate the Wilson loop [42] over the flat bands in Fig. 1(c) which shows no winding (see [41] for the Wilson loops of the dispersive bands). Hence the fragile topology of the flat bands is trivialized by flux. This is possible without a gap closing because the fragile topology of TBG is reliant on $C_{2z}\mathcal{T}$ [12, 15, 43–45], which is broken by flux. The total Chern number of the flat bands is zero, so they cannot be modeled as Landau levels despite the strong flux.

To gain a deeper understanding of the topology at 2π flux, we study the band representation $\mathcal{B}$ with topological quantum chemistry [46–48]. First, Fig. 1b demonstrates that the flat bands remain gapped from all other bands in flux (despite the fragile topology of TBG [8]). Thus $\mathcal{B}$ can be obtained by reducing the band representation of TBG in zero flux derived in Ref. [12] to $p31m'$. We find

$$\mathcal{B} = 2\Gamma_1 + K_2 + K_3 + K_2' + K_3' = A_{2b} \uparrow p31m' \tag{5}$$

which is an elementary band representation and is not topological. The irreps are defined by

$$\begin{array}{c|cc} 3m' & 1 & C_{3z} \\ \hline \Gamma_1 & 1 & 1 \end{array}, \quad \begin{array}{c|cc} 3 & 1 & C_{3z} \\ \hline K_2 & 1 & e^{\frac{2\pi i}{3}} \\ K_3 & 1 & e^{-\frac{2\pi i}{3}} \end{array}, \quad \begin{array}{c|cc} 3 & 1 & C_{3z} \\ \hline K_3' & 1 & e^{\frac{2\pi i}{3}} \\ K_2' & 1 & e^{-\frac{2\pi i}{3}} \end{array} \tag{6}$$

and A_{2b} denotes two irreps of s orbitals at the corners of the moiré unit cell, matching the charge centers at zero flux [10, 12, 49]. Consulting the Bilbao Crystallographic Server, we observe that Eq. (5) is decomposable in momentum space [50–52]. Hence the reduced symmetry group in flux permits the flat bands to be split into disconnected Chern bands given by

$$\mathcal{B} = \mathcal{B}_+ + \mathcal{B}_- = (\Gamma_1 + K_2 + K_3') + (\Gamma_1 + K_3 + K_2') \quad (7)$$

where $\mathcal{B}_\pm$ carries Chern number $C = \pm 1 \mod 3$ [53]. The irreps of $\mathcal{B}_\pm$ at the K and K' points are related by the anti-unitary operator $M\mathcal{T}$ which obeys $C_{3z}M\mathcal{T} = M\mathcal{T}C_{3z}^\dagger$, so Eq. (7) is the only allowed decomposition. We show below that the addition of P, which is not part of the irrep classification (it is not a crystallographic symmetry), forbids this splitting. To split the flat bands, we incorporate the exact θ dependence into the kinetic terms of Eq. (1), breaking P [12, 15] and opening a $\sim .5$meV gap at K and K'. We verify the Chern number decomposition in Eq. (7) from the Wilson loop [41].

Eq. (7) suggests a remarkable similarity to the topology of the flat bands at zero flux, where $C_{2z}\mathcal{T}$ enforces *connected* bands with opposite Chern numbers [12, 15, 43, 44]. We have shown that flux breaks $C_{2z}\mathcal{T}$ and allows the bands to split, yielding strong topology. The flat bands at 2π flux carry opposite Chern numbers, but they cannot annihilate with each other: $M\mathcal{T}$ symmetry ensures any band touching come in pairs so the Chern numbers can only change in multiples of two.

The particle-hole approximation in Eq. (1) prevents the Chern decomposition in Eq. (7) because P and C_{3z} enforce gapless points at K and K' as we now show. Observe that the K and K' points are symmetric under the anti-commuting symmetry $\mathcal{P} = PM\mathcal{T}$ because P takes $\mathbf{k} \to -\mathbf{k}$ and $M\mathcal{T}$ takes $(k_x, k_y) \to (k_x, -k_y)$ [12]. $\mathcal{P}$ is anti-unitary and obeys $C_{3z}\mathcal{P} = \mathcal{P}C_{3z}^\dagger$. As such, a state $|\omega\rangle$ of energy $E \neq 0$ and C_{3z} eigenvalue ω ensures a distinct state $\mathcal{P}|\omega\rangle$ with C_{3z} eigenvalue ω and energy $-E$. Thus all states at $E \neq 0$ come in $\mathcal{P}$-related pairs with the same C_{3z} eigenvalue. Hence if $\mathcal{P}$ is unbroken, the irreps of $\mathcal{B}$ at K and K' are pinned together at $E = 0$ because they have different C_{3z} eigenvalues.

Coulomb Groundstates. Flat bands provide a tractable many-body problem because exact ground states can be obtained for the interaction term while reliably neglecting the competing effects of the kinetic energy after projection [63]. Band topology plays an essential role in this setting. The un-projected Coulomb interaction consists of commuting local operators, but projecting into the flat bands introduces non-triviality due to the wavefunction form factors with a profound effect on the charge excitations [64]. The preceding sections have established TBG at 2π flux as a flat band system with different topology in its wavefunctions due to the breaking of $C_{2z}\mathcal{T}$, serving as a useful comparison to TBG at zero flux.

We now study many-body states where the spin and valley degrees of freedom are important. The low energy states come from the two graphene valleys which we index by $\eta = \pm 1$. The valleys are interchanged by C_{2z} which is unbroken by flux, and hence the flat bands are each four-fold degenerate. To split the degeneracy, we consider adding the interaction

$$H_{int} = \frac{1}{2\Omega_{tot}} \sum_{\mathbf{q}} V(\mathbf{q}) \bar{\rho}_{-\mathbf{q}} \bar{\rho}_{\mathbf{q}}, \quad \bar{\rho}_{\mathbf{q}} = \int d^2r \, e^{-i\mathbf{q}\cdot\mathbf{r}} \bar{n}(\mathbf{r}) \quad (8)$$

where $V(\mathbf{q}) > 0$ is the screened Coulomb potential [54, 55], $\bar{n}(\mathbf{r})$ is the total electron density (summed over valley and spin) measured from charge neutrality, and Ω_{tot} is the area of the sample. In zero flux, the Hamiltonian conserves spin, charge, and valley, so there is an exact $U(2) \times U(2)$ symmetry. It is natural to work in a strong coupling expansion where we project H_{int} onto the two flat bands and neglect their kinetic energy (including particle-hole breaking terms) entirely. This is a very reliable approximation because the bandwidth is ~ 1 meV and the interaction strength is ~ 20meV. In this limit, $C_{2z}P$ commutes with the projected H_{int} operator and the symmetry group is promoted to $U(4)$[54, 56].

We now discuss the fate of the $U(4)$ symmetry in flux. At $B \sim 25$T, the Zeeman effect shifts the energy of the spin $\pm 1/2$ electrons by $\pm \mu_B B = \pm 1.4$meV where μ_B is the Bohr magneton. This shift is comparable to the bandwidth, so it is consistent to neglect both at leading order. (The Zeeman term will choose the spin-polarized states out of the $U(4)$ manifold.) We should also consider twist angle homogeneity which has recently come under scrutiny [57–59]. Experiments indicate that even in high quality devices, the moiré twist angle θ varies locally up to $.1^\circ$ [60–62], leading to local variations in the unit cell and hence the flux. In a realistic sample with domains of varying θ at constant B, we expect deviations from the 2π flux flat band wavefunctions. However, the large interaction strength and gap to the passive bands still makes the strong coupling expansion appropriate.

An analytic study of the strong-coupling problem is possible because H_{int} is positive semi-definite [63]. Following Ref. [64], we study exact eigenstates at fillings $\nu = 0, 2, 4$ ($-\nu$ follows from many-body particle-hole symmetry [54]) and derive the excitation spectrum, effectively determining the complete renormalization of the flat bands by the Coulomb interaction. Ref. [64] was also able to study odd ν perturbatively using the chiral symmetry at $w_0 = 0$ [13, 14, 16, 65]. The chiral limit at 2π flux is topologically distinct [65] from the physical regime $w_0/w_1 = .6$ - $.8$ (unlike at zero flux) so this approach is inapplicable. Odd fillings are left to future work.

The many-body calculation at 2π flux is tractable using a gauge-invariant expression for H_{int} and the form factors. Following Ref. [66], we produce exact many-body insulator eigenstates of the projected H_{int} at even ν:

$$|\Psi_\nu\rangle = \prod_{\mathbf{k}} \prod_{j}^{(4+\nu)/2} \gamma^\dagger_{\mathbf{k},+,\eta_j,s_j} \gamma^\dagger_{\mathbf{k},-,\eta_j,s_j} |0\rangle \quad (9)$$

where $\gamma^\dagger_{\mathbf{k},M,\eta,s}$ creates a state at momentum $\mathbf{k}$, valley η, and spin s in the $M = \pm 1$ band. The states $|\Psi_\nu\rangle$ fully occupy the two flat bands for arbitrary η_j, s_j forming a

$U(4)$ multiplet. Including valley and spin, there are 8 flat bands; $|\Psi_\nu\rangle$ fills $(4+\nu)/2$ of them. At $\nu=0$, $|\Psi_0\rangle$ must be a groundstate because H_{int} is positive semi-definite and $H_{int}|\Psi_0\rangle = 0$. At $\nu=\pm 4$ where the system is a band insulator, $|\Psi_{\pm 4}\rangle$ are trivially groundstates because they are completely empty/occupied. The $|\Psi_{\pm 2}\rangle$ states are exact eigenstates, and we argue they are groundstates using the flat metric condition (FMC) [66] which assumes the Hartree potential of the flat bands is trivial. Ref. [54] found that the FMC holds reliably at zero flux, and we check that the FMC is similarly reliable at 2π flux [39]. Like at zero flux, $|\Psi_\nu\rangle$ has Chern number zero, but without $C_{2z}\mathcal{T}$ there is no fragile topology.

The exact eigenstates $|\Psi_\nu\rangle$ enable us to compute the charge excitation spectrum at filling ν. The Hamiltonian $R^\eta_+(\mathbf{k})$ governing the $+1$ charge spectrum is defined

$$[H_{int}-\mu N, \gamma^\dagger_{\mathbf{k},M,s,\eta}]\,|\Psi_\nu\rangle \equiv \frac{1}{2}\sum_N \gamma^\dagger_{\mathbf{k},N,s,\eta}[R^\eta_+(\mathbf{k})]_{NM}\,|\Psi_\nu\rangle \tag{10}$$

where η, s are *unoccupied* indices in $|\Psi_\nu\rangle$ and μ is the chemical potential [41]. Counting the flavors in Eq. (9), at filling ν the charge ± 1 excitations come in multiples of $(4\mp\nu)/2$. A direct calculation of $R^\eta_\pm(\mathbf{k})$, the ± 1 charge excitation Hamiltonian, is possible thanks to our gauge-invariant expression for the form factors in flux. Performing the commutators at $\nu=0$ in Eq. (10) gives [41]

$$R_+(\mathbf{k}) = \sum_{\mathbf{q}} \frac{V(\mathbf{q})}{\Omega_{tot}} M^\dagger(\mathbf{k},\mathbf{q})M(\mathbf{k},\mathbf{q}) \tag{11}$$

and the form factor matrices in the flat bands are

$$M(\mathbf{k},\mathbf{q}) = e^{i\xi_{\mathbf{q}}(\mathbf{k})}U^\dagger(\mathbf{k}-\mathbf{q})\mathcal{H}^{\mathbf{q}}U(\mathbf{k}) \tag{12}$$

where $\mathcal{H}^{\mathbf{q}} = e^{i\epsilon_{ij}q_i\tilde{Z}_j}$ is a unitary matrix acting on the Landau level indices like in the Berry connection (see Eq. (4)) and $e^{i\xi_{\mathbf{q}}(\mathbf{k})}$ can be expressed in terms of Siegel theta functions [41]. Eq. (11) demonstrates that the excitations at $\nu=0$ are governed by the wavefunctions $U(\mathbf{k})$ (like at zero flux) as well as $\mathcal{H}^{\mathbf{q}}$, a new factor intrinsic to magnetic flux. The phase factor $e^{i\xi_{\mathbf{q}}(\mathbf{k})}$ cancels in Eq. (11) at $\nu=0$, but contributes nontrivially at $\nu=\pm 2$ [41]. Next, because $V(\mathbf{q})>0$ and $M^\dagger M$ is a positive definite matrix, we see that $R_\pm(\mathbf{k})$ is positive definite and thus describes gapped excitations (an insulator). Lastly, we observe that all $\mathbf{k}$ dependence in $R_\pm(\mathbf{k})$ comes from the wavefunctions, so the dispersion of the excitation bands depends the non-triviality of $U(\mathbf{k})$. For example, in the decoupled Landau limit where $U(\mathbf{k})$ is independent of $\mathbf{k}$ and nonzero only for a single Landau level n, $R_\pm(\mathbf{k})$ has exactly flat bands. We plot the excitation spectrum at $\nu=0$ and $\nu=2$ in Fig. 2, observing significant dispersion since, as shown by irreps Eq. (5), TBG at 2π flux is far from the Landau level regime.

The dispersion of the excitations leaves distinctive signatures in the Landau fans emanating from the $|\Psi_\nu\rangle$ insulators [11, 29, 67]. At $\nu=0$, the ± 1 charge excitations are identical and their dispersion features a charge gap to a band with a quadratic minima at the Γ point. Hence at low densities, there are $(4\mp 0)/2=2$ massive quasi-particles, counting the degenerate charge excitations in different spin-valley flavors. As the flux is increased, the massive quadratic excitations form Landau levels (quantum Hall states), leading to Landau fans away from $\nu=0$ in multiples of 2 — half the Landau level degeneracy of TBG near $B=0$. The gap between the two excitation bands at Γ depends on w_0/w_1. Fig. 2a shows the generic case at $w_0/w_1=.71$, but at $w_0/w_1=.8$ the two bands are nearly degenerate at Γ [41]. At $\nu=2$, the -1 excitation (towards charge neutrality) has a large mass which reduces the gap between Landau levels and masks would-be insulating states. However, the $+1$ excitation has a smaller effective mass and will create Landau levels in multiples of $(4-2)/2=1$. We do not discuss excitations above $\nu=4$ here because they fill the passive bands, and we check that the charge -1 excitation below $\nu=4$ (not shown) is gapped with a very large mass. We note that at zero flux with $C_{2z}\mathcal{T}$, the excitation bands must be degenerate at the Γ point [64, 68]. Based on the $U(4)$ symmetry which determines the $(4\mp\nu)/2$ degeneracy of the excitations, the breaking of $C_{2z}\mathcal{T}$ which allows the bands to be gapped at Γ, and the large mass of excitations towards charge neutrality, we predict the Landau fans emerging from $\nu=0$ and $\nu=2$ away from charge neutrality to have degeneracies 2 and 1 respectively.

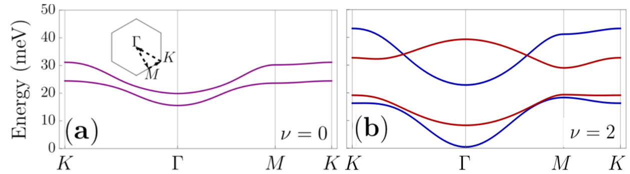

FIG. 2. $\frac{1}{2}R^\eta_\pm(\mathbf{k})$ spectra at $w_0/w_1=.71$. (a) At $\nu=0$, the charge ± 1 excitations are identical and feature a quadratic (massive) dispersion at the Γ point. (b) At $\nu=2$, the charge -1 excitation (red) has a large mass, strongly suppressing the Landau fans pointing towards charge neutrality, while the $+1$ excitation (blue) is lighter by a factor of 3. The $+1$ charge gap at $\nu=2$ is $\sim$ .5meV or roughly 5K.

Discussion. We used an exact method to study TBG at 2π flux, yielding comprehensive results for the single-particle and many-body physics. Recently, interest in reentrant superconductivity and correlated phases in strong flux has invigorated research in moiré materials [69–71]. Our formalism makes it possible to study such phenomena with the tools of modern band theory and without recourse to approximate models. We find that the emblematic topological flat bands and correlated insulators of TBG are re-entrant at $\phi=2\pi$, providing strong evidence that magic-angle physics recurs at ~ 25T. The excitation spectrum at $\nu=2$ reveals dispersive quasi-particles away from charge neutrality as at zero flux (but with half the degeneracy due to $C_{2z}\mathcal{T}$ breaking). This leads us to conjecture that superconductivity, which occurs at $\phi = 0$ upon doping correlated insulating states, may also be reentrant at 2π flux [40].

Acknowledgements. We thank Zhi-Da Song for early insight and Luis Elcoro for useful discussions. B.A.B. and A.C. were supported by the ONR Grant No. N00014-20-1-2303, DOE Grant No. DESC0016239, the Schmidt Fund for Innovative Research, Simons Investigator Grant No. 404513, the Packard Foundation, the Gordon and Betty Moore Foundation through Grant No. GBMF8685 towards the Princeton theory program, and a Guggenheim Fellowship from the John Simon Guggenheim Memorial Foundation. Further support was provided by the NSF-MRSEC Grant No. DMR-1420541 and DMR-2011750, BSF Israel US foundation Grant No. 2018226, and the Princeton Global Network Funds. JHA is supported by a Marshall Scholarship funded by the Marshall Aid Commemoration Commission.

Note added. During the publication of this work, Ref. [72] appeared which investigated reentrant single-particle flat bands in TBG using a tight-binding model on very large commensurate unit cell. Their findings are consistent with our continuum approach when both valleys are included.

[1] Yuan Cao, Valla Fatemi, Ahmet Demir, Shiang Fang, Spencer L. Tomarken, Jason Y. Luo, Javier D. Sanchez-Yamagishi, Kenji Watanabe, Takashi Taniguchi, Efthimios Kaxiras, Ray C. Ashoori, and Pablo Jarillo-Herrero. Correlated insulator behaviour at half-filling in magic-angle graphene superlattices. *Nature (London)*, 556(7699):80–84, Apr 2018. doi:10.1038/nature26154.

[2] Yuan Cao, V. Fatemi, S. Fang, K. Watanabe, T. Taniguchi, E. Kaxiras, and P. Jarillo-Herrero. Unconventional superconductivity in magic-angle graphene superlattices. *Nature*, 556:43–50, 2018.

[3] Kyounghwan Kim, Ashley DaSilva, Shengqiang Huang, Babak Fallahazad, Stefano Larentis, Takashi Taniguchi, Kenji Watanabe, Brian J. LeRoy, Allan H. MacDonald, and Emanuel Tutuc. Tunable moiré bands and strong correlations in small-twist-angle bilayer graphene. *Proceedings of the National Academy of Sciences*, 114(13):3364–3369, 2017. ISSN 0027-8424. doi:10.1073/pnas.1620140114. URL `https://www.pnas.org/content/114/13/3364`.

[4] Dante M. Kennes, Martin Claassen, Lede Xian, Antoine Georges, Andrew J. Millis, James Hone, Cory R. Dean, D. N. Basov, Abhay N. Pasupathy, and Angel Rubio. Moiré heterostructures as a condensed-matter quantum simulator. *Nature Physics*, 17(2):155–163, January 2021. doi:10.1038/s41567-020-01154-3.

[5] Leon Balents, Cory R Dean, Dmitri K Efetov, and Andrea F Young. Superconductivity and strong correlations in moiré flat bands. *Nature Physics*, 16(7):725–733, 2020.

[6] Jianpeng Liu and Xi Dai. Orbital magnetic states in moiré graphene systems. *Nature Reviews Physics*, pages 1–16, 2021.

[7] Yanbang Chu, Le Liu, Yalong Yuan, Cheng Shen, Rong Yang, Dongxia Shi, Wei Yang, and Guangyu Zhang. A review of experimental advances in twisted graphene moiré superlattice. *Chinese Physics B*, 29(12):128104, dec 2020. doi:10.1088/1674-1056/abb221. URL `https://doi.org/10.1088/1674-1056/abb221`.

[8] Jonah Herzog-Arbeitman, Zhi-Da Song, Nicolas Regnault, and B. Andrei Bernevig. Hofstadter topology: Noncrystalline topological materials at high flux. *Phys. Rev. Lett.*, 125:236804, Dec 2020. doi:10.1103/PhysRevLett.125.236804. URL `https://link.aps.org/doi/10.1103/PhysRevLett.125.236804`.

[9] Rafi Bistritzer and Allan H. MacDonald. Moiré bands in twisted double-layer graphene. *Proceedings of the National Academy of Science*, 108(30):12233–12237, Jul 2011. doi:10.1073/pnas.1108174108.

[10] Mikito Koshino, Noah F. Q. Yuan, Takashi Koretsune, Masayuki Ochi, Kazuhiko Kuroki, and Liang Fu. Maximally localized wannier orbitals and the extended hubbard model for twisted bilayer graphene. *Phys. Rev. X*, 8:031087, Sep 2018. doi:10.1103/PhysRevX.8.031087. URL `https://link.aps.org/doi/10.1103/PhysRevX.8.031087`.

[11] Ipsita Das, Xiaobo Lu, Jonah Herzog-Arbeitman, Zhi-Da Song, Kenji Watanabe, Takashi Taniguchi, B. Andrei Bernevig, and Dmitri K. Efetov. Symmetry-broken Chern insulators and Rashba-like Landau-level crossings in magic-angle bilayer graphene. *Nature Physics*, 17(6): 710–714, January 2021. doi:10.1038/s41567-021-01186-3.

[12] Zhi-Da Song, Zhijun Wang, Wujun Shi, Gang Li, Chen Fang, and B. Andrei Bernevig. All Magic Angles in Twisted Bilayer Graphene are Topological. *Phys. Rev. Lett.*, 123(3):036401, Jul 2019. doi: 10.1103/PhysRevLett.123.036401.

[13] Grigory Tarnopolsky, Alex Jura Kruchkov, and Ashvin Vishwanath. Origin of magic angles in twisted bilayer graphene. *Phys. Rev. Lett.*, 122:106405, Mar 2019. doi: 10.1103/PhysRevLett.122.106405. URL `https://link.aps.org/doi/10.1103/PhysRevLett.122.106405`.

[14] B. Andrei Bernevig, Zhi-Da Song, Nicolas Regnault, and Biao Lian. Twisted bilayer graphene. I. Matrix elements, approximations, perturbation theory, and a k .p two-band model. *Phys. Rev. B*, 103(20):205411, May 2021. doi:10.1103/PhysRevB.103.205411.

[15] Zhi-Da Song, Biao Lian, Nicolas Regnault, and B. Andrei Bernevig. Twisted bilayer graphene. II. Stable symmetry anomaly. *Phys. Rev. B*, 103(20):205412, May 2021. doi: 10.1103/PhysRevB.103.205412.

[16] Jie Wang, Yunqin Zheng, Andrew J. Millis, and Jennifer Cano. Chiral Approximation to Twisted Bilayer Graphene: Exact Intra-Valley Inversion Symmetry, Nodal Structure and Implications for Higher Magic Angles. *arXiv e-prints*, art. arXiv:2010.03589, October 2020.

[17] Bin-Bin Chen, Yuan Da Liao, Ziyu Chen, Oskar Vafek, Jian Kang, Wei Li, and Zi Yang Meng. Realization of Topological Mott Insulator in a Twisted Bilayer Graphene Lattice Model. *arXiv e-prints*, art. arXiv:2011.07602, November 2020.

[18] Liujun Zou, Hoi Chun Po, Ashvin Vishwanath, and T. Senthil. Band structure of twisted bilayer graphene:

Emergent symmetries, commensurate approximants, and wannier obstructions. *Phys. Rev. B*, 98:085435, Aug 2018. doi:10.1103/PhysRevB.98.085435. URL https://link.aps.org/doi/10.1103/PhysRevB.98.085435.

[19] Douglas R. Hofstadter. Energy levels and wave functions of bloch electrons in rational and irrational magnetic fields. *Phys. Rev. B*, 14:2239–2249, Sep 1976. doi:10.1103/PhysRevB.14.2239.

[20] Jian Wang and Luiz H. Santos. Classification of topological phase transitions and van hove singularity steering mechanism in graphene superlattices. *Phys. Rev. Lett.*, 125:236805, Dec 2020. doi:10.1103/PhysRevLett.125.236805. URL https://link.aps.org/doi/10.1103/PhysRevLett.125.236805.

[21] C. Albrecht, J. H. Smet, K. von Klitzing, D. Weiss, V. Umansky, and H. Schweizer. Evidence of hofstadter's fractal energy spectrum in the quantized hall conductance. *Phys. Rev. Lett.*, 86:147–150, Jan 2001. doi:10.1103/PhysRevLett.86.147. URL https://link.aps.org/doi/10.1103/PhysRevLett.86.147.

[22] B. Andrei Bernevig and Taylor L. Hughes. *Topological Insulators and Topological Superconductors*. Princeton University Press, student edition edition, 2013. ISBN 9780691151755.

[23] Xiaobo Lu, Biao Lian, Gaurav Chaudhary, Benjamin A. Piot, Giulio Romagnoli, Kenji Watanabe, Takashi Taniguchi, Martino Poggio, Allan H. MacDonald, B. Andrei Bernevig, and Dmitri K. Efetov. Fingerprints of Fragile Topology in the Hofstadter spectrum of Twisted Bilayer Graphene Close to the Second Magic Angle. *PNAS*, art. arXiv:2006.13963, June 2020.

[24] C. R. Dean, L. Wang, P. Maher, C. Forsythe, F. Ghahari, Y. Gao, J. Katoch, M. Ishigami, P. Moon, M. Koshino, T. Taniguchi, K. Watanabe, K. L. Shepard, J. Hone, and P. Kim. Hofstadter's butterfly and the fractal quantum hall effect in moirésuperlattices. *Nature*, 497:598 EP –, 05 2013.

[25] J. Zak. Magnetic translation group. *Phys. Rev.*, 134:A1602–A1606, Jun 1964. doi:10.1103/PhysRev.134.A1602. URL https://link.aps.org/doi/10.1103/PhysRev.134.A1602.

[26] J. Zak. Magnetic translation group. ii. irreducible representations. *Phys. Rev.*, 134:A1607–A1611, Jun 1964. doi:10.1103/PhysRev.134.A1607. URL https://link.aps.org/doi/10.1103/PhysRev.134.A1607.

[27] E. Brown. Aspects of group theory in electron dynamics**this work supported by the u.s. atomic energy commission. 22:313–408, 1969. ISSN 0081-1947. doi:https://doi.org/10.1016/S0081-1947(08)60033-8. URL https://www.sciencedirect.com/science/article/pii/S0081194708600338.

[28] P Streda. Theory of quantised hall conductivity in two dimensions. *Journal of Physics C: Solid State Physics*, 15(22):L717–L721, aug 1982. doi:10.1088/0022-3719/15/22/005. URL https://doi.org/10.1088/0022-3719/15/22/005.

[29] G. H. Wannier. A Result Not Dependent on Rationality for Bloch Electrons in a Magnetic Field. *Physica Status Solidi B Basic Research*, 88(2):757–765, August 1978. doi:10.1002/pssb.2220880243.

[30] Daniela Pfannkuche and Rolf R. Gerhardts. Theory of magnetotransport in two-dimensional electron systems subjected to weak two-dimensional superlattice potentials. *Phys. Rev. B*, 46:12606–12626, Nov 1992. doi:10.1103/PhysRevB.46.12606. URL https://link.aps.org/doi/10.1103/PhysRevB.46.12606.

[31] Tong zhong Li, Ke lin Wang, and Jinlong Yang. Thermal properties of a two-dimensional electron gas under a one-dimensional periodic magnetic field. *Journal of Physics: Condensed Matter*, 9:9299–9313, 1997.

[32] J. Milton Pereira, F. M. Peeters, and P. Vasilopoulos. Landau levels and oscillator strength in a biased bilayer of graphene. *Phys. Rev. B*, 76:115419, Sep 2007. doi:10.1103/PhysRevB.76.115419. URL https://link.aps.org/doi/10.1103/PhysRevB.76.115419.

[33] Di Xiao, Ming-Che Chang, and Qian Niu. Berry phase effects on electronic properties. *Rev. Mod. Phys.*, 82:1959–2007, Jul 2010. doi:10.1103/RevModPhys.82.1959. URL https://link.aps.org/doi/10.1103/RevModPhys.82.1959.

[34] Godfrey Gumbs, Desiré Miessein, and Danhong Huang. Effect of magnetic modulation on bloch electrons on a two-dimensional square lattice. *Phys. Rev. B*, 52:14755–14760, Nov 1995. doi:10.1103/PhysRevB.52.14755. URL https://link.aps.org/doi/10.1103/PhysRevB.52.14755.

[35] R. Bistritzer and A. H. MacDonald. Moiré butterflies in twisted bilayer graphene. *Phys. Rev. B*, 84:035440, Jul 2011. doi:10.1103/PhysRevB.84.035440. URL https://link.aps.org/doi/10.1103/PhysRevB.84.035440.

[36] Kasra Hejazi, Chunxiao Liu, and Leon Balents. Landau levels in twisted bilayer graphene and semiclassical orbits. *Phys. Rev. B*, 100(3):035115, July 2019. doi:10.1103/PhysRevB.100.035115.

[37] J. A. Crosse, Naoto Nakatsuji, Mikito Koshino, and Pilkyung Moon. Hofstadter butterfly and the quantum hall effect in twisted double bilayer graphene. *Physical Review B*, 102(3), Jul 2020. ISSN 2469-9969. doi:10.1103/physrevb.102.035421. URL http://dx.doi.org/10.1103/PhysRevB.102.035421.

[38] Biao Lian, Fang Xie, and B. Andrei Bernevig. Open momentum space method for the Hofstadter butterfly and the quantized Lorentz susceptibility. *Phys. Rev. B*, 103(16):L161405, April 2021. doi:10.1103/PhysRevB.103.L161405.

[39] Jonah Herzog-Arbeitman, Aaron Chew, and B. Andrei Bernevig. Magnetic Bloch Theorem and Reentrant Flat Bands in Twisted Bilayer Graphene at 2π Flux. *arXiv e-prints*, art. arXiv:2206.07717, June 2022.

[40] Ipsita Das, Cheng Shen, Alexandre Jaoui, Jonah Herzog-Arbeitman, Aaron Chew, Chang-Woo Cho, Kenji Watanabe, Takashi Taniguchi, Benjamin A. Piot, B. Andrei Bernevig, and Dmitri K. Efetov. Observation of reentrant correlated insulators and interaction driven fermi surface reconstructions at one magnetic flux quantum per moiré unit cell in magic-angle twisted bilayer graphene.

[41] See supplementary materials for a description of additional calculations.

[42] A. Alexandradinata, Xi Dai, and B. Andrei Bernevig. Wilson-Loop Characterization of Inversion-Symmetric Topological Insulators. *Phys. Rev.*, B89(15):155114, 2014. doi:10.1103/PhysRevB.89.155114.

[43] Jianpeng Liu, Junwei Liu, and Xi Dai. Pseudo landau level representation of twisted bilayer graphene: Band topology and implications on the correlated insulating phase. *Phys. Rev. B*, 99:155415, Apr 2019. doi:10.1103/PhysRevB.99.155415. URL https://link.aps.org/doi/10.1103/PhysRevB.99.155415.

[44] J. Ahn, S. Park, and B.-J. Yang. Failure of Nielsen-Ninomiya Theorem and Fragile Topology in Two-Dimensional Systems with Space-Time Inversion Symmetry: Application to Twisted Bilayer Graphene at Magic Angle. *Physical Review X*, 9(2):021013, April 2019. doi: 10.1103/PhysRevX.9.021013.

[45] Adrien Bouhon, Annica M. Black-Schaffer, and Robert-Jan Slager. Wilson loop approach to fragile topology of split elementary band representations and topological crystalline insulators with time-reversal symmetry. *Phys. Rev. B*, 100(19):195135, November 2019. doi: 10.1103/PhysRevB.100.195135.

[46] Barry Bradlyn, L. Elcoro, Jennifer Cano, M. G. Vergniory, Zhijun Wang, C. Felser, M. I. Aroyo, and B. Andrei Bernevig. Topological quantum chemistry. *Nature (London)*, 547(7663):298–305, Jul 2017. doi: 10.1038/nature23268.

[47] MI Aroyo, JM Perez-Mato, Cesar Capillas, Eli Kroumova, Svetoslav Ivantchev, Gotzon Madariaga, Asen Kirov, and Hans Wondratschek. Bilbao crystallographic server: I. databases and crystallographic computing programs. *ZEITSCHRIFT FUR KRISTALLOGRAPHIE*, 221:15–27, 01 2006. doi: 10.1524/zkri.2006.221.1.15.

[48] Mois I. Aroyo, Asen Kirov, Cesar Capillas, J. M. Perez-Mato, and Hans Wondratschek. Bilbao Crystallographic Server. II. Representations of crystallographic point groups and space groups. *Acta Crystallographica Section A*, 62(2):115–128, Mar 2006. doi: 10.1107/S0108767305040286.

[49] Jian Kang and Oskar Vafek. Symmetry, Maximally Localized Wannier States, and a Low-Energy Model for Twisted Bilayer Graphene Narrow Bands. *Physical Review X*, 8(3):031088, July 2018. doi: 10.1103/PhysRevX.8.031088.

[50] Jennifer Cano, Barry Bradlyn, Zhijun Wang, L. Elcoro, M. G. Vergniory, C. Felser, M. I. Aroyo, and B. Andrei Bernevig. Topology of Disconnected Elementary Band Representations. *Phys. Rev. Lett.*, 120(26):266401, June 2018. doi:10.1103/PhysRevLett.120.266401.

[51] Jennifer Cano, Barry Bradlyn, Zhijun Wang, L. Elcoro, M. G. Vergniory, C. Felser, M. I. Aroyo, and B. Andrei Bernevig. Building blocks of topological quantum chemistry: Elementary band representations. *Phys. Rev. B*, 97 (3):035139, Jan 2018. doi:10.1103/PhysRevB.97.035139.

[52] Barry Bradlyn, Zhijun Wang, Jennifer Cano, and B. Andrei Bernevig. Disconnected elementary band representations, fragile topology, and wilson loops as topological indices: An example on the triangular lattice. *Physical Review B*, 99(4), Jan 2019. ISSN 2469-9969. doi: 10.1103/physrevb.99.045140. URL `http://dx.doi.org/10.1103/PhysRevB.99.045140`.

[53] Chen Fang, Matthew J. Gilbert, and B. Andrei Bernevig. Bulk topological invariants in noninteracting point group symmetric insulators. *Phys. Rev. B*, 86(11):115112, September 2012. doi:10.1103/PhysRevB.86.115112.

[54] B. Andrei Bernevig, Zhi-Da Song, Nicolas Regnault, and Biao Lian. Twisted bilayer graphene. III. Interacting Hamiltonian and exact symmetries. *Phys. Rev. B*, 103(20):205413, May 2021. doi: 10.1103/PhysRevB.103.205413.

[55] Xiaoxue Liu, Zhi Wang, K. Watanabe, T. Taniguchi, Oskar Vafek, and J. I. A. Li. Tuning electron correlation in magic-angle twisted bilayer graphene using Coulomb screening. *Science*, 371(6535):1261–1265, March 2021. doi:10.1126/science.abb8754.

[56] Oskar Vafek and Jian Kang. Towards the hidden symmetry in Coulomb interacting twisted bilayer graphene: renormalization group approach. *arXiv e-prints*, art. arXiv:2009.09413, September 2020.

[57] Justin H. Wilson, Yixing Fu, S. Das Sarma, and J. H. Pixley. Disorder in twisted bilayer graphene. *Phys. Rev. Research*, 2:023325, Jun 2020. doi: 10.1103/PhysRevResearch.2.023325. URL `https://link.aps.org/doi/10.1103/PhysRevResearch.2.023325`.

[58] Daniel E. Parker, Tomohiro Soejima, Johannes Hauschild, Michael P. Zaletel, and Nick Bultinck. Strain-induced quantum phase transitions in magic angle graphene. *arXiv e-prints*, art. arXiv:2012.09885, December 2020.

[59] Bikash Padhi, Apoorv Tiwari, Titus Neupert, and Shinsei Ryu. Transport across twist angle domains in moiré graphene. *arXiv e-prints*, art. arXiv:2005.02406, May 2020.

[60] A. Uri, S. Grover, Y. Cao, J. Â. A. Crosse, K. Bagani, D. Rodan-Legrain, Y. Myasoedov, K. Watanabe, T. Taniguchi, P. Moon, M. Koshino, P. Jarillo-Herrero, and E. Zeldov. Mapping the twist-angle disorder and Landau levels in magic-angle graphene. *Nature (London)*, 581(7806):47–52, May 2020. doi:10.1038/s41586-020-2255-3.

[61] Nathanael P. Kazmierczak, Madeline Van Winkle, Colin Ophus, Karen C. Bustillo, Hamish G. Brown, Stephen Carr, Jim Ciston, Takashi Taniguchi, Kenji Watanabe, and D. Kwabena Bediako. Strain fields in twisted bilayer graphene. *arXiv e-prints*, art. arXiv:2008.09761, August 2020.

[62] Tjerk Benschop, Tobias A. de Jong, Petr Stepanov, Xiaobo Lu, Vincent Stalman, Sense Jan van der Molen, Dmitri K. Efetov, and Milan P. Allan. Measuring local moiré lattice heterogeneity of twisted bilayer graphene. *Phys. Rev. Research*, 3:013153, Feb 2021. doi:10.1103/PhysRevResearch.3.013153. URL `https://link.aps.org/doi/10.1103/PhysRevResearch.3.013153`.

[63] Jian Kang and Oskar Vafek. Strong coupling phases of partially filled twisted bilayer graphene narrow bands. *Phys. Rev. Lett.*, 122:246401, Jun 2019. doi: 10.1103/PhysRevLett.122.246401. URL `https://link.aps.org/doi/10.1103/PhysRevLett.122.246401`.

[64] B. Andrei Bernevig, Biao Lian, Aditya Cowsik, Fang Xie, Nicolas Regnault, and Zhi-Da Song. Twisted bilayer graphene. V. Exact analytic many-body excitations in Coulomb Hamiltonians: Charge gap, Goldstone modes, and absence of Cooper pairing. *Phys. Rev. B*, 103(20): 205415, May 2021. doi:10.1103/PhysRevB.103.205415.

[65] Yarden Sheffer and Ady Stern. Chiral Magic-Angle Twisted Bilayer Graphene in a Magnetic Field: Landau Level Correspondence, Exact Wavefunctions and Fractional Chern Insulators. *arXiv e-prints*, art. arXiv:2106.10650, June 2021.

[66] Biao Lian, Zhi-Da Song, Nicolas Regnault, Dmitri K. Efetov, Ali Yazdani, and B. Andrei Bernevig. Twisted bilayer graphene. IV. Exact insulator ground states and phase diagram. *Phys. Rev. B*, 103(20):205414, May 2021. doi:10.1103/PhysRevB.103.205414.

[67] Biao Lian, Fang Xie, and B. Andrei Bernevig. The

Landau Level of Fragile Topology. *arXiv e-prints*, art. arXiv:1811.11786, November 2018.

[68] Jian Kang, B. Andrei Bernevig, and Oskar Vafek. Cascades between light and heavy fermions in the normal state of magic angle twisted bilayer graphene. *arXiv e-prints*, art. arXiv:2104.01145, April 2021.

[69] Gaurav Chaudhary, A. H. MacDonald, and M. R. Norman. Quantum Hall Superconductivity from Moir{é} Landau Levels. *arXiv e-prints*, art. arXiv:2105.01243, May 2021.

[70] Yuan Cao, Jeong Min Park, Kenji Watanabe, Takashi Taniguchi, and Pablo Jarillo-Herrero. Large Pauli Limit Violation and Reentrant Superconductivity in Magic-Angle Twisted Trilayer Graphene. *arXiv e-prints*, art. arXiv:2103.12083, March 2021.

[71] Daniel Shaffer, Jian Wang, and Luiz H. Santos. Theory of Hofstadter superconductors. *Phys. Rev. B*, 104(18):184501, November 2021. doi: 10.1103/PhysRevB.104.184501.

[72] Yifei Guan, Oleg V. Yazyev, and Alexander Kruchkov. Re-entrant magic-angle phenomena in twisted bilayer graphene in integer magnetic fluxes. *arXiv e-prints*, art. arXiv:2201.13062, January 2022.